ADVANCED QUANTUM TECHNOLOGIES
www.advquantumtech.com

Optical Signatures of Defect Centers in Transition Metal Dichalcogenide Monolayers

Pedro Miguel M. C. de Melo, Zeila Zanolli, and Matthieu J. Verstraete*

Even the best quality 2D materials have non-negligible concentrations of vacancies and impurities. It is critical to understand and quantify how defects change intrinsic properties, and use this knowledge to generate functionality. This challenge can be addressed by employing many-body perturbation theory to obtain the optical absorption spectra of defected transition metal dichalcogenides. Herein metal vacancies, which are largely unreported, show a larger set of polarized excitons than chalcogenide vacancies, introducing localized excitons in the sub-optical-gap region, whose wave functions and spectra make them good candidates as quantum emitters. Despite the strong interaction with substitutional defects, the spin texture and pristine exciton energies are preserved, enabling grafting and patterning in optical detectors, as the full optical-gap region remains available. A redistribution of excitonic weight between the A and B excitons is visible in both cases and may allow the quantification of the defect concentration. This work establishes excitonic signatures to characterize defects in 2D materials and highlights vacancies as qubit candidates for quantum computing.

Transition metal dichalcogenides (TMDs) have become strong contenders for the engineering of optical devices, especially thanks to their coupling of the spin and valley degrees of freedom, and the presence of strongly bound excitons, opening avenues for next generation opto-electronics.[1,2] Manufactured samples have strongly improved in quality, but will always contain a significant concentration of defects.[3,4] Graphene can be crystallized almost perfectly in very large flakes, but TMDs present many more natural defects, in particular chalcogen vacancies (see e.g., Ref. [5]). On the bright side, defects and substitutional dopants can be used to tune the electronic structure and optical properties of materials.[6] By doing so, devices sensitive to specific wavelengths and polarizations can be engineered (reviewed in Ref. [7]), and can even behave as single photon emitters.[8] There is an ongoing search for long lived spin states at room temperatures in TMDs. Here defects are expected to play a crucial role in both scattering and storing spin information - we showed recently that intrinsic scattering mechanisms (the electron-phonon interaction) can quickly destroy the pumped spin-polarization.[9] Chalcogen vacancies can also be used as grafting sites for functional groups, to create bio and chemical sensors.[10,11] Alkane and other functional groups can be incorporated directly into the matrix (as opposed to thiol links, for instance, which necessitate Au). Carbon atoms have also been used as acceptor dopants for bulk semiconductors.[12] In TMDs, mixed phases with transition metal carbides have been shown to have applications in catalysis,[13,14] while in MoS_2 it was shown that carbon substitutions had a strong effect on the TMD electronic and optical properties.[15,16]

Many experiments give access to the presence and properties of localized defects. In TMDs the most commonly used are: scanning tunneling microscopy which shows contrast changes due to chemical substitution and electron cloud reconstruction around defects;[17] scanning tunneling spectroscopy, which probes the detailed electronic structure at the defect site;[17] optical spectroscopy showing absorption and photoluminescence by the defect-induced states;[18–20] tunneling transport from insulated contacts through a core material, which is resonant through defect states in the core band gap;[19] transmission electron microscopy, which gives both structural and chemical information.[3,21]

Understanding how defects affect optical properties is a first essential step toward controlled functionalization of materials, both for fingerprinting (optical characterization is simple, remote, and non-destructive) and to understand derived optical functionalities. First-principles computational techniques

Dr. P. M. M. C. de Melo, Prof. M. J. Verstraete
nanomat/Q-mat/CESAM
Université de Liège
Institut de Physique
B-4000 Sart Tilman, Liège, Belgium
E-mail: p.m.monteirocamposdemelo@uu.nl
Dr. P. M. M. C. de Melo, Prof. Z. Zanolli
Chemistry Department
Debye Institute for Nanomaterials Science
Condensed Matter and Interfaces
Utrecht University
PO Box 80.000, 3508 TA Utrecht, The Netherlands
Prof. Z. Zanolli
Catalan Institute of Nanoscience and Nanotechnology (ICN2)
CSIC and BIST
Campus UAB, Bellaterra, Barcelona 08193, Spain
Dr. P. M. M. C. de Melo, Prof. Z. Zanolli, Prof. M. J. Verstraete
European Theoretical Spectroscopy Facility (ETSF) www.etsf.eu

The ORCID identification number(s) for the author(s) of this article can be found under https://doi.org/10.1002/qute.202000118

DOI: 10.1002/qute.202000118

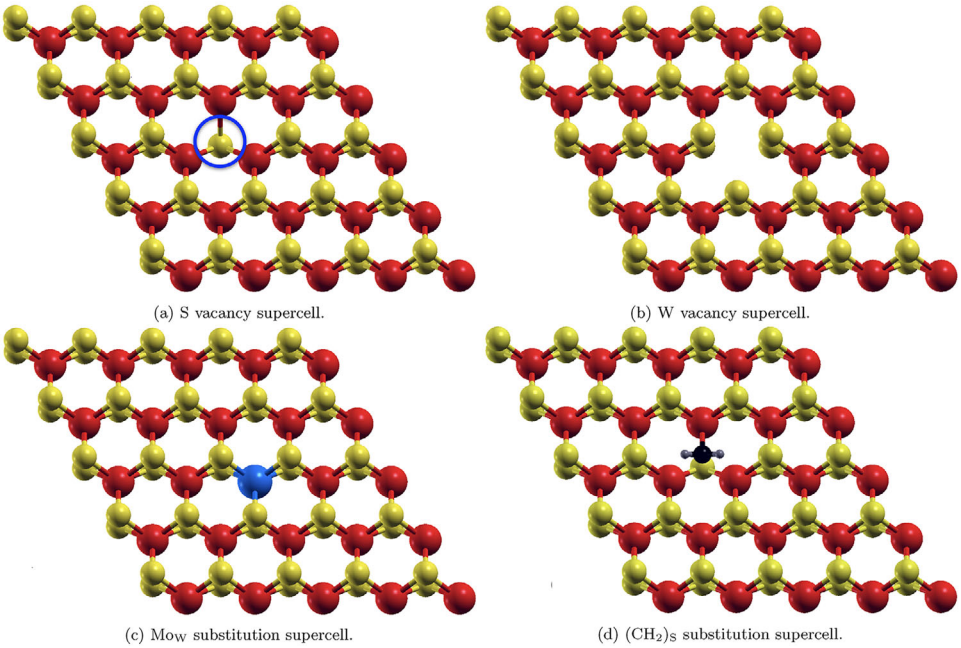

Figure 1. Defected 5×5 supercells used in this work. a) S vacancy, marked by the blue circle. b) W vacancy. c) Mo_W substitution. d) $(CH_2)_S$ substitution. Tungsten atoms are shown in red, sulfur in yellow, molybdenum in blue, carbon in black, and hydrogen in grey.

provide a high degree of physical insight and predictive power in the spectral features of defects, to find new peaks and yield quantitative positions and weight transfers.

Several methods can be used to generate defects in layers of TMDs: in situ defects can be created by either chemical vapor transport (CVT) or chemical vapor deposition, which allow for some degree of control in the generation of substitutional defects or chalcogenide vacancies during the synthesis of the system; techniques such as electron beam irradiation, ion bombardment, plasma treatment, thermal annealing, ozone treatment, and laser illumination can be used to create ex situ defects.[7] The four point defects we present in this work, S vacancy, W vacancy, Mo_W substitution, $(CH_2)_S$ substitution, are thus a representative sample of different systems that can be of interest in the near future. While some studies on the optical response of defected TMD supercells exist,[22–24] here we present a representative sample of highly converged calculations on defects that have shown potential due to their ease in manufacturing (S vacancy, Mo_W substitution, $(CH_2)_S$ substitution) or rich optical features (W vacancy). However, multiple types of point defects can be present in the sample, coming from the synthesis process or subsequent treatments. If these defects add new states to the mid-gap region, it could complicate the identification of defects from optical measurements, depending on their line-widths and experimental resolution. Further research should look into the most common defects introduced during sample treatment after synthesis and their effects on optical response.

In this work, we present a fully First-principles investigation of charge-neutral defected monolayers of WS_2, based on the Bethe–Salpeter equation (BSE) for electron–hole interactions within many body perturbation theory. In Ref. [22] it has been shown that charging a defect in TMDs mainly changes the absolute energies of defect states, but almost not their number or their relative gaps. Since bulk states are the dominant contribution to electronic screening, we expect that our results are also indicative of the behavior of charged defects. We analyze the resulting changes in electronic band structure and optical absorption spectra, aiming to answer the question: can we identify a defect, and ideally quantify its concentration,[22] just by looking at the absorption spectrum? While chalcogen vacancies have been subject to some studies,[22] metal vacancies and isovalent substitutions like Mo_W and $(CH_2)_S$ are still largely unreported, limiting our knowledge of their behavior as quantum emitters or chemical detectors. We find that defects fall into two functional categories, based on the presence of bound states within the band-gap of WS_2. We discuss their spectra, spin textures and the criteria which could be used to identify each defect.

In **Figure 1** we show the four defects that are the focus of our work: two vacancies (S and W ions); and two substitutions, Mo_W and $(CH_2)_S$. The S vacancy is the most commonly found defect in monolayers of WS_2 and often assigned to specific features below the optical gap.[18] In the substitution case Mo_W is quite commonly found in nature, and carbon is a common dopant in semiconductors.[25] Studies have been made on the potential transport applications of TMDs and transition metal carbides.[13,26] In the case of MoS_2 experiments point to changes to the electronic structure due to carbon doping, which should translate into new optical features.[15,27]

In ideal defect engineering, induced changes in the system should yield new controllable features that are distinct from the pristine properties. In the case of TMDs, a key property that relates to optics is the polarization of states at the K wave vector in the Brillouin zone. The polarization will control the allowed optical transitions that form bright excitons. We label in order of increasing energy the last two occupied states and the first two unoccupied states at K as (v_1, v_2, c_1, c_2). For pristine WS_2 (see the

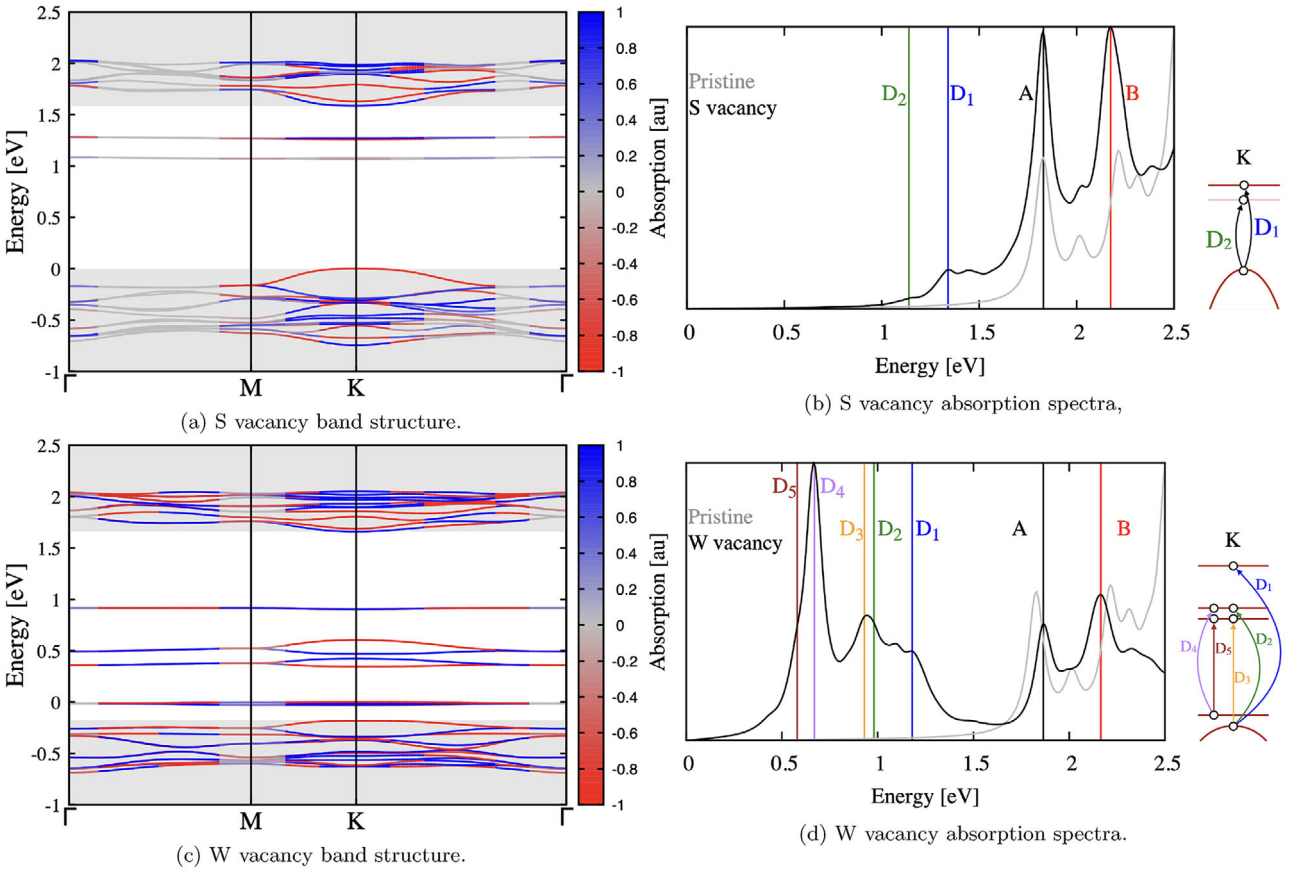

(a) S vacancy band structure.

(b) S vacancy absorption spectra,

(c) W vacancy band structure.

(d) W vacancy absorption spectra.

Figure 2. a,c) DFT band structures and spin-texture of defected WS_2 for the S and W vacancies, respectively. Color scale indicates value of $\langle S_z \rangle$ (red for 1 and blue for −1). The Fermi level is set to the last occupied state and shaded regions indicate the bulk region. In both cases new states arise in the mid-gap region. Two occupied defect states are visible in the band structure of the W vacancy. b,d) Optical absorption spectra of the S and W vacancies, respectively. The spectra are cut at 2.5 eV, as higher energy bands were not included in the BSE kernel. Calculations were converged to reproduce A and B bulk exciton peaks. Absorption of the pristine system is shown in grey. The positions of the first excitonic peaks are shown by vertical lines. Labels and vertical lines have matching colors. Two new peaks arise for the S vacancy due to the two new manifolds of mid-gap states. The W vacancy exhibits several new peaks, as four new manifolds of defect states arise. The outsets in (b) and (d) show the level scheme and main excitonic transitions.

Supporting Information for more information), the first bright exciton would be made of an optical transition from v_2 to c_2, while the second brightest exciton would be made by a transition from v_1 to c_1. This is due to the fact that optical selection rules enforce spin conservation in TMDs: the valence and conduction manifold differ in orbital character, guaranteeing the needed angular momentum change when absorbing a helical photon.[28]

We start by analyzing two systems which feature states in the pristine band gap: the sulfur and tungsten vacancies. Their DFT band structures are shown in **Figure 2**a,c, respectively. Note that using a 5×5 supercell, the point K of the pristine Brillouin zone (BZ) folds back into the point K of the supercell BZ.

Both systems preserve the spin polarization of pristine states at K, meaning that the A and B peaks that are the dominant features of the pristine spectrum must also be present. For the S vacancy, Figure 2a, new non-dispersive mid-gap singlet states appear 1.08 and 1.28 eV above the valence band edge, in agreement with what was previously found.[16,29] At K the first band is almost completely spin-unpolarized, while the second is completely polarized. This opens a path for new emission channels, as electronic transitions from the pristine valence states to these new defect states are allowed, with different oscillator strengths and different excitation energies.

The W vacancy is more challenging numerically: the defect bands are split off from the bulk conduction and valence bands, but in the 5×5 supercell they still show some dispersion and a finite band width. Their position and spin texture are close to what has been found in other DFT calculations for this defect using larger supercells,[16] and we extract a semi-quantitative picture of the optical properties. Together with the six new mid-gap states, there are also four new occupied states bound to the defect in the valence region (unlike the S vacancy). All these states are spin polarized at K, so if we consider optical selection rules, we can expect new peaks to show up in the absorption spectrum. These peaks will be a combination of transitions between pristine and defect states, and others between defect states (occupied to empty) in the mid-gap region.

The effects of changes in the band structure on the BSE optical spectrum are shown in Figure 2. For comparison the absorption spectrum of the pristine system is shown in grey. The energies of all identified excitons are listed in Table S1, Supporting Information, along with the reference energies for the pristine case.

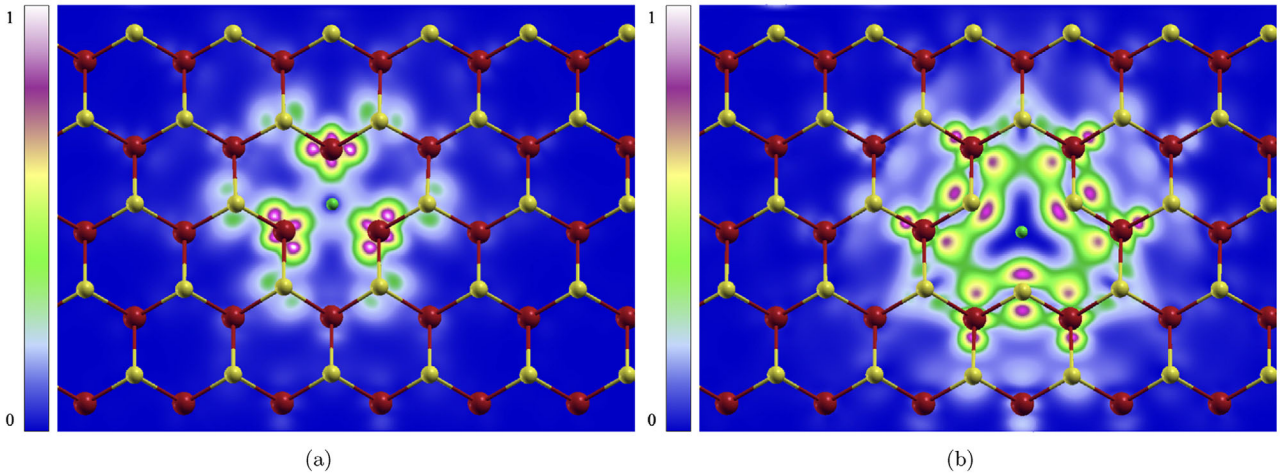

Figure 3. a) S vacancy wave function for excitonic state D_2, shown in Figure 2b. b) W vacancy wave function for excitonic state D_5, shown in Figure 2d. The hole is marked by the green sphere and it is placed at the position of the missing sulfur ion. In both cases the electronic charge is highly localized near the hole, indicating the formation of a quantum dot.

Note in passing that the higher energy peaks beyond A and B are not reproduced in full in our calculations, due to limitations in the number of states included in the BSE for such large systems.

With an S vacancy in Figure 2a two new peaks arise at 1.35 and 1.14 eV due to the mid-gap states. They are marked D_1 and D_2 in Figure 2b. As shown in the inset, D_1 and D_2 correspond to optical transitions from the top valence band to the defect state at 1.28 and 1.08 eV, respectively. However, since the lowest defect state is not fully polarized, the resulting dipole matrix element is much smaller than that of the D_1 peak, where the defect state is fully polarized.

The exciton wave function for the peak corresponding to D_1 is shown in **Figure 3**a. Here the hole is placed at the position of the vacant sulfur ion (marked by the green sphere) and the magnitude on the color-map shows the probability density of the electron (see the Figure S5, Supporting Information where all the excitonic wave functions are depicted). The color map shows that exciton states are highly localized on the neighboring tungsten atoms, indicating that the S vacancy does indeed form a quantum dot.

For the W vacancy, whose spectrum is shown in Figure 2d, more peaks are present due to the increased number of defect states. In total we identify five excitons: three composed from holes in the valence band and electrons in defect states, D_1 to D_3; and two others with both the electron and the hole bound to two different manifolds of defect states, D_4 and D_5. The states involved in the formation in the excitons are shown in the inset of Figure 2d. The most striking feature is the relative intensity of the D_4 and D_5 excitons relative to the A and B excitons. As defect states have very weak dispersion, the associated electrons and holes will have large effective masses. It is possible to show[30] that oscillator strengths are proportional to the reduced mass of electron and hole, which explains why the effect is further magnified for transitions between defect states in the case of the W vacancy.

The high intensity shown in Figure 2d for exciton states D_3, D_4, and D_5 is an artifact and results mainly from the overlapping of the Lorentzian functions used to plot the peaks associated with each exciton. For D_3 and D_5, their relative intensities with respect to exciton A are 0.47 and 0.76, respectively. For the exciton state D_4, the relative intensity is 1.88. However, this exciton state still suffers from contaminating interactions coming from adjacent vacancy sites, resulting from the size of the supercell used in our calculations. Table S2, Supporting Information shows all the relative intensities of each exciton state with respect to the A exciton for all systems.

A more detailed analysis to the excitonic wave functions shows that two of the low intensity peaks (D_1 and D_3) are artifacts due to the interaction of defect states in neighboring periodic replicas. They result from electron-hole pairs localized on different vacancy sites (see Figure S7, Supporting Information for zoomed out plots of excitonic wave function). The majority of the electronic charge in the exciton is not localized near the same ion vacancy as the hole, and is bound thanks to a finite overlap of the DFT defect state wavefunctions. These two peaks will disappear if larger supercells are used: the dipole matrix element and oscillator strength will go do 0. We note that while the BSE is solved only for $\mathbf{q} = 0$, the introduction of non-dispersive defect states allows for many transitions to occur throughout the BZ, so an exciton function can actually be composed of several vertical transitions at different momenta (NB: this is distinct from a finite wave vector for the whole exciton).

In the case of D_2, shown in Figure S7, Supporting Information, there is a residual interaction with adjacent vacancy sites, but now the hole is correctly bound to an electron located at the same site. For D_5, shown in Figure 3b both the electron and hole are entirely located at the same site.

We note that hybridization between bulk and defect exciton states is not expected to occur in systems with low defect density. In the case of our calculations all wave-functions are orthogonal by construction, and for larger supercells any overlap between pristine and defect excitons should vanish.

The two vacancies thus show very distinct optical signatures, coming from the different richness in defect states that arise in their band structures. This, together with the changes in the intensity due to different levels of defect density (see

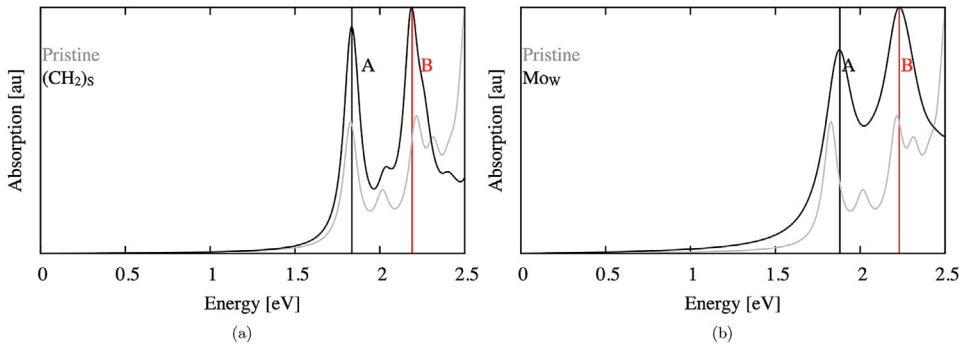

Figure 4. Optical absorption spectra for the 5×5 supercells with the a) $(CH_2)_S$ substitution; b) MoS_2 substitution. Absorption of the pristine system is shown in grey. The positions of the first excitonic peaks are shown by vertical lines. Labels and vertical lines have matching colors. Both cases show no new peaks, with the A and B excitons at energies that almost match those of the pristine case. The spectra are cut at 2.5 eV, as higher energy bands were not included in the BSE kernel. Calculations were converged to reproduce the A and B bulk exciton peaks.

Figure S10, Supporting Information) indicate that even at low densities it should be possible to distinguish between a sulfur and a tungsten vacancy just through measuring the optical absorption of the sample.

We studied two cases of substitutions in the WS_2 monolayer; one with a molybdenum atom replacing a tungsten atom; and another where a sulfur atom was replaced by a methyl, the simplest (divalent) group representing grafted organic substituents.

In both cases no mid gap states where found (see Figure S4, Supporting Information for their bandstructures), which can be rationalized as follows. In the case of Mo_W substitution, molybdenum and tungsten have the same valence, close atomic and covalent radii,[31–33] resulting in similar chemical properties. A small concentration of defects does not lead to strong changes in the charge density, thus leaving the system practically unchanged when compared to the pristine case. For the $(CH_2)_S$ substitution, the methylene group provides the same number of valence electrons as the sulfur atom. The breaking of local symmetry is not strong enough to perturb the band edges.

The lack of mid-gap states is reflected in the absorption spectra shown in **Figure 4**. In both cases the excitonic peaks lie almost on top of those of the pristine system, with the largest deviation being 60 meV for the Mo_W A peak. The energies for the defected A and B peaks are shown in Table S1, Supporting Information.

There is, however, both weight transfer and changes in spin texture for the A and B peaks at higher energies in the absorption spectrum of both substitutions, which leaves some hope to identify these defects experimentally. The strongest signature of the substitution lies within the exciton wave functions shown in **Figure 5**. While the exciton cloud is still dispersed throughout the crystal, there is a higher charge concentration near the substitution. In the $(CH_2)_S$ case this is valid for the A exciton (Figure 5c), and in Mo_W both A and B excitonic states localize near the defect. The $(CH_2)_S$ case also shows breaking of C_3 symmetry by the methyl molecule. The localization is due both to the defect-related electronic states and to the choice of the initial position of the hole. For reference, in boron nitride similar extensions of 3–5 nearest neighbors are found in Ref. [34].

The two peaks which correspond to the bulk excitons A and B known from literature, and are within 50 meV of those of the pristine system in all cases (this is below the absolute precision of the first principles methods, and shows the basic convergence of our supercell sizes). If experimental precision is on this level the main spectral signature for Mo_W is the blue shift of the A peak and the broadening of both peaks. However, many other (especially isovalent) defects may have similar manifestations.

We can now establish a more complete picture of how different defects change optical properties of TMDs. The main changes to the optical spectrum come from new mid-gap states. Isovalent substitutions like Mo_W and $(CH_2)_S$ will not be trivially seen in the absorption spectra, but can still be detected by the ratio of the A and B peak intensities, and by localization in the exciton's spatial distribution.

In terms of potential applications, the two vacancies are clear front runners for designing quantum dots and quantum emitters. In particular the S vacancy has already shown some promising results as a single photon emitter.[35] The two mid-gap defect states are actively considered for quantum computing applications: they are separated in energy by 0.21 eV, making them addressable using mid-infrared lasers, and insulating them from the highest phonon energy in pristine WS_2, which is 53 meV.[36,37]

The W vacancy offers a larger set of localized excitons, but is more energetic and harder to produce (see Table S1, Supporting Information). Here the brightest excitons are made of transitions between single particle defect states, due to their large effective masses. These exciton states show potential in devices as they would behave as bright emitters with multiple internal states, behaving like an embedded molecule for multivalued quantum computing.[38] The residual band width will disappear only in a 7×7 supercell,[16] but the spin texture and qualitative features are already well represented here (see Figure S3, Supporting Information). In actual samples, this vacancy type is more likely to be charged, with electrons filling the dangling S ion's orbitals.

We have shown that the isovalent substitutions Mo_W and $(CH_2)_S$ will not produce in-gap states. Though this is intuitive, it is not trivial, and the local electronic structure is strongly modified as shown by the excitonic wave functions. For purposes of grafting organic molecules, this means the full band gap window of intrinsic WS_2 will be available for optical sensing.

In conclusion, we employ powerful and accurate first principles techniques to shed some light into the changes in optical properties introduced by point defects in TMDs. Two promising systems, S and W ion vacancies, have potential for quantum

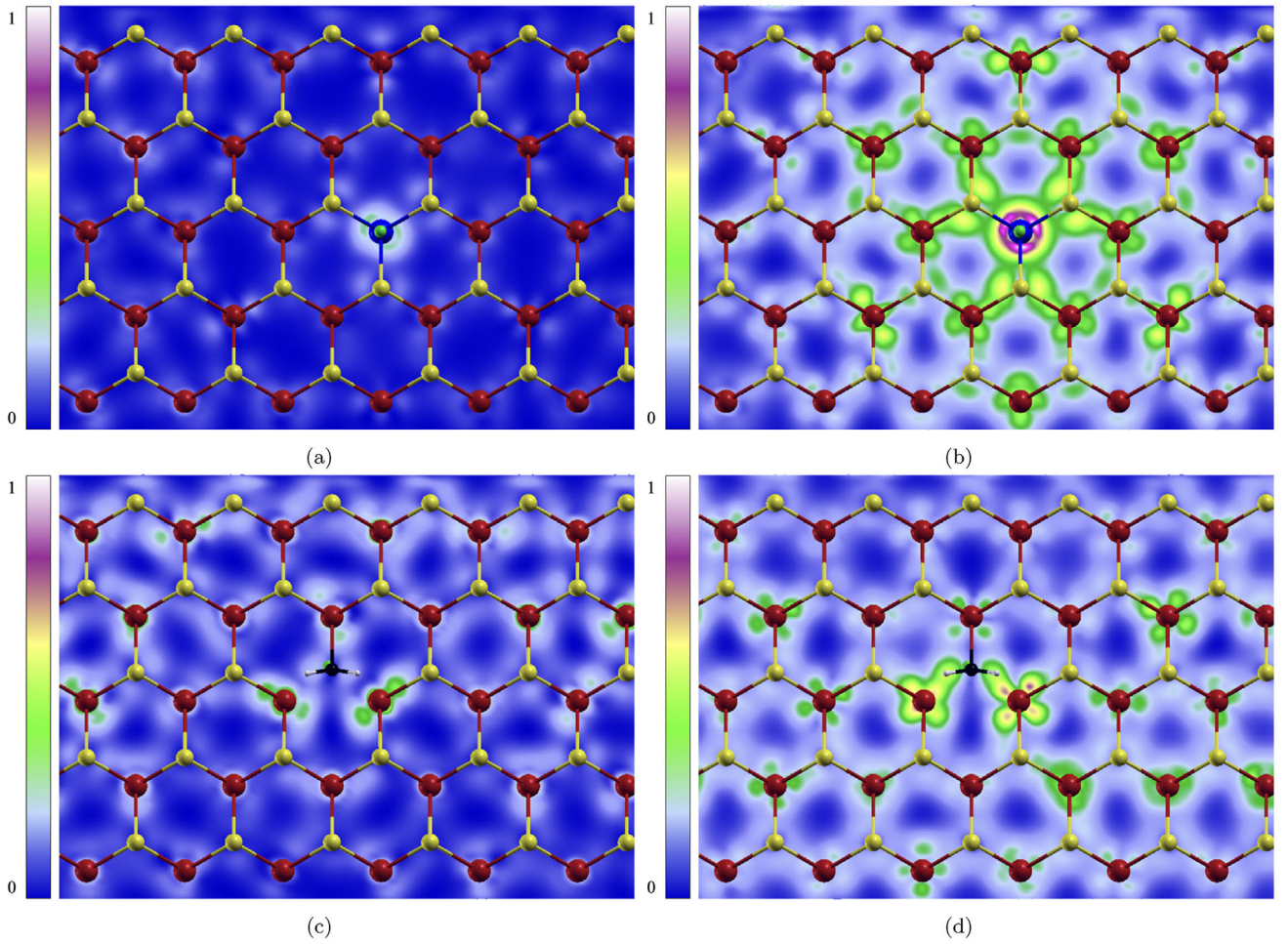

Figure 5. The A (left column) and B (right) excitonic wave functions of a,b) Mo_W and c,d) $(CH_2)_S$, shown in Figure 4. The hole is marked by the green sphere and it is placed between the mid-plane and the carbon ion. While there is some charge localization and symmetry breaking, the exciton wave function extends through the whole system.

emitters and even quantum computing. While W vacancies are the least energetically favorable, it is the one with the richest and most interesting variety of defect bound excitons. Such defects might be possible to synthesize in environments with lower concentrations of tungsten or focused TEM beams. Isovalent vacancies do not introduce mid-gap states in the band structure, but do change the relative intensity of the canonical A and B peaks, and the spatial distribution of the first and second excitonic states, in the $(CH_2)_S$ case even leading to a breaking of symmetry. In both cases the full sub optical gap region is available for use in detection of molecules that might graft themselves onto the TMD's surface.

Methodology Section

Ground state calculations and structural optimization were performed with the Quantum Espresso package[39] using the GGA exchange correlation functional. Supercells where generated by replicating the pristine cell (previously optimized) and then introducing a defect. The electrostatic isolation in the out-of-plane direction was ensured by a Coulomb cutoff technique.[40] A plane-wave kinetic energy cutoff of 95 Ry was used, with a tolerance parameter of 10^{-12} for the error in the density. The forces on the atoms were converged down to 10^{-5} Ry bohr^{-1} and the minimum difference in total energies was set to 10^{-8} Ry to achieve structural optimization. The pristine systems were computed on a 30×30 k-point mesh. Therefore, a mesh of 6×6 k-points was sufficient for modeling the 5×5 supercells.

G_0W_0 corrections of the ground state electronic structure were computed in the plasmon–pole approximation, using the `Yambo` code.[41] A total of 1700 bands where necessary to converge the screening, while kinetic cut-offs of 2 Ha where used to compute the integrals. This allowed for convergence within the range of the meV. The resulting energy level corrections were then used in solving the BSE equation, as shown in Equation (1).

The absorption spectra was computed using the Bethe–Salpeter equation[42] as implemented in the `Yambo` code,[41] to properly account for excitonic effects. This involves solving the eigenvalue equation

$$\left(\varepsilon^{GW}_{c\mathbf{k}} - \varepsilon^{GW}_{v\mathbf{k}}\right) A^{\lambda}_{vc\mathbf{k}} + \sum_{\mathbf{k}'c'v'} K^{eh}_{\substack{vc\mathbf{k} \\ v'c'\mathbf{k}'}} A^{\lambda}_{v'c'\mathbf{k}'} = E_{\lambda} A^{\lambda}_{vc\mathbf{k}} \quad (1)$$

where $\varepsilon_{c\mathbf{k}/v\mathbf{k}}$ are quasi-particle band energies obtained from the G_0W_0 COHSEX approximation[42] and K^{eh} accounts for the static screened and bare Coulomb interactions between electrons and holes. The excitonic wave function, $|\lambda\rangle$, is then constructed by using

$$|\lambda\rangle = \sum_{\mathbf{k},c,v} A^{\lambda}_{vc\mathbf{k}} \, |c\mathbf{k}\rangle \, |v\mathbf{k}\rangle \tag{2}$$

In the calculations the focus is on the bound exciton energies below the band gap, so the BSE kernel only has the electron–hole pairs needed to converge the pristine system's first two excitons, marked as A and B. The optical absorption was then obtained directly from the imaginary part of the dielectric function, $\varepsilon(\omega)$, which is given (within the Tamm–Dancoff approximation) by

$$\varepsilon(\omega) = -2 \lim_{\mathbf{q}\to 0} \sum_{\lambda,c,v,\mathbf{k}} \frac{\left| \langle v\mathbf{k} - \mathbf{q} | e^{-i\mathbf{q}\cdot\mathbf{r}} | c\mathbf{k} \rangle \, A^{\lambda}_{cv\mathbf{k}} \right|^2}{\omega - E_{\lambda} + i\eta} \tag{3}$$

Here c/v represent conduction/valence states, $\mathbf{k}$ is the k-point vector in the Brillouin zone. λ, E_{λ}, and $A^{\lambda}_{cv\mathbf{k}}$ are the exciton index, eigenenergy and eigenvector of Equation 1. The electron–hole interaction is included in K^{eh}, which contains both the un-screened exchange interaction and the screened direct Coulomb interaction. The values for kinetic cut-off parameters were equal to those used during the GW-COHSEX calculations. In order to properly account for the bands in the same energy range as the pristine case, a total of 60 bands were used in the BSE kernel.

Supporting Information

Supporting Information is available from the Wiley Online Library or from the author.

Acknowledgements

The authors wish to acknowledge important input, discussions, and stimulus from M. Terrones, B. Biel, and M. Palummo, as well as extensive support from the Yambo developer team.

P.M.M.C.M. and M.J.V. acknowledge funding by the Belgian FNRS (PDR G.A. T.1077.15, T.0103.19, and an "out" sabbatical grant to ICN2 Barcelona), and the Communauté Française de Belgique (ARC AIMED G.A. 15/19-09). This publication is based upon work of the MELODICA project, funded by the EU FLAG-ERA_JTC2017 call. The work benefited from HPC-EUROPA3 (INFRAIA-2016-1-730897) H2020 Research Innovation Action hosted by the Theory and Simulation group at ICN2 supported by the Barcelona Supercomputing Center, and from the access provided by ICN2 (Barcelona, Spain) within the framework of the NFFA-Europe Transnational Access Activity (grant agreement No 654360, proposal ID 717, submitted by PMMCM). Z.Z. acknowledges support by the Ramón y Cajal program RYC-2016-19344 (MINECO/AEI/FSE, UE), Spanish MINECO (FIS2015-64886-C5-3-P), the Severo Ochoa Program (MINECO, SEV-2017-0706), the CERCA programme of the Generalitat de Catalunya (Grant 2017SGR1506), the EC H2020-INFRAEDI-2018-2020 MaX Materials Design at the Exascale CoE(grant No. 824143), and the Netherlands sector plan program 2019–2023. Computational resources were provided by the Consortium des Equipements de Calcul Intensif (CECI), funded by FRS-FNRS G.A. 2.5020.11; the Zenobe Tier-1 supercomputer funded by Walloon G.A. 1117545; and by PRACE DECI grants 2DSpin and Pylight on Beskow (G.A. 653838 of H2020, and FP7 RI-312763). The authors thankfully acknowledge the computer resources at Mare Nostrum technical support provided by the Barcelona Supercomputing Center (Spanish Supercomputing Network, RES). This publication is also based upon work from COST Action TUMIEE (CA17126), supported by COST (European Cooperation in Science and Technology).

Conflict of Interest

The authors declare no conflict of interest.

Keywords

defect centers, optical absorption, transition metal dichalcogenides, quantum dots

Received: October 15, 2020
Revised: December 7, 2020
Published online: February 3, 2021

[1] Q. H. Wang, K. Kalantar-Zadeh, A. Kis, J. N. Coleman, M. S. Strano, *Nat. Nanotechnol.* **2012**, *7*, 699.
[2] K. F. Mak, J. Shan, *Nat. Photonics* **2016**, *10*, 216.
[3] D. Edelberg, D. Rhodes, A. Kerelsky, B. Kim, J. Wang, A. Zangiabadi, C. Kim, A. Abhinandan, J. Ardelean, M. Scully, D. Scullion, L. Embon, R. Zu, E. J. G. Santos, L. Balicas, C. Marianetti, K. Barmak, X. Zhu, J. Hone, A. N. Pasupathy, *Nano Lett.* **2019**, *19*, 4371.
[4] N. Briggs, S. Subramanian, Z. Lin, X. Li, X. Zhang, K. Zhang, K. Xiao, D. Geohegan, R. Wallace, L.-Q. Chen, M. Terrones, A. Ebrahimi, S. Das, J. Redwing, C. Hinkle, K. Momeni, A. van Duin, V. Crespi, S. Kar, J. A. Robinson, *2D Mater.* **2019**, *6*, 022001.
[5] H.-P. Komsa, J. Kotakoski, S. Kurasch, O. Lehtinen, U. Kaiser, A. V. Krasheninnikov, *Phys. Rev. Lett.* **2012**, *109*, 035503.
[6] S. Feng, Z. Lin, X. Gan, R. Lv, M. Terrones, *Nanoscale Horiz.* **2017**, *2*, 72.
[7] Z. Lin, B. R. Carvalho, E. Kahn, R. Lv, R. Rao, H. Terrones, M. A. Pimenta, M. Terrones, *2D Mater.* **2016**, *3*, 022002.
[8] R. Bourrellier, S. Meuret, A. Tararan, O. Stéphan, M. Kociak, L. H. Tizei, A. Zobelli, *Nano Lett.* **2016**, *16*, 4317.
[9] M. Ersfeld, F. Volmer, P. M. M. C. de Melo, R. de Winter, M. Heithoff, Z. Zanolli, C. Stampfer, M. J. Verstraete, B. Beschoten, *Nano Lett.* **2019**, *19*, 4083.
[10] A. Bolotsky, D. Butler, C. Dong, K. Gerace, N. R. Glavin, C. Muratore, J. A. Robinson, A. Ebrahimi, *ACS Nano* **2019**, *13*, 9781.
[11] J. Azadmanjiri, P. Kumar, V. K. Srivastava, Z. Sofer, *ACS Appl. Nano Mater.* **2020**, *3*, 3116.
[12] L. W. Yang, P. D. Wright, V. Eu, Z. H. Lu, A. Majerfeld, *J. Appl. Phys.* **1992**, *72*, 2063.
[13] Z. Hai, J. Du, M. K. Akbari, C. Xue, H. Xu, S. Zhuiykov, *Ionics* **2017**, *23*, 1921.
[14] J. Wu, L. Ma, A. Samanta, M. Liu, B. Li, Y. Yang, J. Yuan, J. Zhang, Y. Gong, J. Lou, R. Vajtai, B. Yakobson, A. K. Singh, C. S. Tiwary, P. M. Ajayan, *Adv. Mater. Interfaces* **2017**, *4*, 1600866.
[15] Q. Yue, S. Chang, S. Qin, J. Li, *Phys. Lett. A* **2013**, *377*, 1362.
[16] M. A. Khan, M. Erementchouk, J. Hendrickson, M. N. Leuenberger, *Phys. Rev. B* **2017**, *95*, 245435.
[17] B. Schuler, J.-H. Lee, C. Kastl, K. A. Cochrane, C. T. Chen, S. Refaely-Abramson, S. Yuan, E. van Veen, R. Roldán, N. J. Borys, R. J. Koch, S. Aloni, A. M. Schwartzberg, D. F. Ogletree, J. B. Neaton, A. Weber-Bargioni, *ACS Nano* **2019**, *13*, 10520.
[18] V. Carozo, Y. Wang, K. Fujisawa, B. R. Carvalho, A. McCreary, S. Feng, Z. Lin, C. Zhou, N. Perea-López, A. L. Elías, B. Kabius, V. H. Crespi, M. Terrones, *Sci. Adv.* **2017**, *3*, e1602813.

[19] T. Y. Jeong, H. Kim, S.-J. Choi, K. Watanabe, T. Taniguchi, K. J. Yee, Y.-S. Kim, S. Jung, *Nat. Commun.* **2019**, *10*, 3825.
[20] J. Dang, S. Sun, X. Xie, Y. Yu, K. Peng, C. Qian, S. Wu, F. Song, J. Yang, S. Xiao, L. Yang, Y. Wang, M. A. Rafiq, C. Wang, X. Xu, *npj 2D Mater. Appl.* **2020**, *4*, 2.
[21] J. Hong, R. Senga, T. Pichler, K. Suenaga, *Phys. Rev. Lett.* **2020**, *124*, 87401.
[22] S. Refaely-Abramson, D. Y. Qiu, S. G. Louie, J. B. Neaton, *Phys. Rev. Lett.* **2018**, *121*, 167402.
[23] F. Zhang, Y. Lu, D. S. Schulman, T. Zhang, K. Fujisawa, Z. Lin, Y. Lei, A. LauraElias, S. Das, S. B. Sinnott, M. Terrones, *Sci. Adv.* **2019**, *5*, 5.
[24] J. Jiang, R. Pachter, S. Mou, *Nanoscale* **2018**, *10*, 13751.
[25] Y. J. Zheng, Y. Chen, Y. L. Huang, P. K. Gogoi, M.-Y. Li, L.-J. Li, P. E. Trevisanutto, Q. Wang, S. J. Pennycook, A. T. S. Wee, S. Y. Quek, *ACS Nano* **2019**, *13*, 6050.
[26] J. Jeon, Y. Park, S. Choi, J. Lee, S. S. Lim, B. H. Lee, Y. J. Song, J. H. Cho, Y. H. Jang, S. Lee, *ACS Nano* **2018**, *12*, 338.
[27] A.-M. Hu, L.-l. Wang, W.-Z. Xiao, G. Xiao, Q.-Y. Rong, *Comput. Mater. Sci.* **2015**, *107*, 72.
[28] A. Molina-Sánchez, D. Sangalli, L. Wirtz, A. Marini, *Nano Lett.* **2017**, *17*, 4549.
[29] B. Schuler, D. Y. Qiu, S. Refaely-Abramson, C. Kastl, C. T. Chen, S. Barja, R. J. Koch, D. F. Ogletree, S. Aloni, A. M. Schwartzberg, J. B. Neaton, S. G. Louie, A. Weber-Bargioni, *Phys. Rev. Lett.* **2019**, *123*, 76801.
[30] C. Hamaguchi, *Basic Semiconductor Physics*, Springer, Cham **2017**.
[31] B. Cordero, V. Gómez, A. E. Platero-Prats, M. Revés, J. Echeverría, E. Cremades, F. Barragán, S. Alvarez, *Dalton Trans.* **2008**, 2832.
[32] P. Pyykkö, M. Atsumi, *Chem. - Eur. J.* **2009**, *15*, 12770.
[33] P. Pyykkö, M. Atsumi, *Chem. - Eur. J.* **2009**, *15*, 186.
[34] F. Paleari, T. Galvani, H. Amara, F. Ducastelle, A. Molina-Sánchez, L. Wirtz, *2D Mater.* **2018**, *5*, 45017.
[35] Y. M. He, G. Clark, J. R. Schaibley, Y. He, M. C. Chen, Y. J. Wei, X. Ding, Q. Zhang, W. Yao, X. Xu, C. Y. Lu, J. W. Pan, *Nat. Nanotechnol.* **2015**, *10*, 497.
[36] N. A. Pike, A. Dewandre, B. Van Troeye, X. Gonze, M. J. Verstraete, *Phys. Rev. Mater.* **2018**, *2*, 63608.
[37] N. A. Pike, A. Dewandre, B. Van Troeye, X. Gonze, M. J. Verstraete, *Phys. Rev. Mater.* **2019**, *3*, 74009.
[38] B. Fresch, M. V. Klymenko, R. D. Levine, F. Remacle, in *Computational Matter* (Eds. S. Stepney, S. Rasmussen, M. Amos), Springer, Cham **2018**, pp. 295–318.
[39] P. Giannozzi, O. Andreussi, T. Brumme, O. Bunau, M. Buongiorno Nardelli, M. Calandra, R. Car, C. Cavazzoni, D. Ceresoli, M. Cococcioni, N. Colonna, I. Carnimeo, A. Dal Corso, S. de Gironcoli, P. Delugas, R. A. DiStasio, A. Ferretti, A. Floris, G. Fratesi, G. Fugallo, R. Gebauer, U. Gerstmann, F. Giustino, T. Gorni, J. Jia, M. Kawamura, H.-Y. Ko, A. Kokalj, E. Küçükbenli, M. Lazzeri, et al., *J. Phys.: Condens. Matter* **2017**, *29*, 465901.
[40] C. A. Rozzi, D. Varsano, A. Marini, E. K. U. Gross, A. Rubio, *Phys. Rev. B* **2006**, *73*, 205119.
[41] D. Sangalli, A. Ferretti, H. Miranda, C. Attaccalite, I. Marri, E. Cannuccia, P. Melo, M. Marsili, F. Paleari, A. Marrazzo, G. Prandini, P. Bonfà, M. O. Atambo, F. Affinito, M. Palummo, A. Molina-Sánchez, C. Hogan, M. Grüning, D. Varsano, A. Marini, *J. Phys.: Condens. Matter* **2019**, *31*, 325902.
[42] G. Onida, L. Reining, A. Rubio, *Rev. Mod. Phys.* **2002**, *74*, 601.